

Observable Signatures of Classical T Tauri Stars Accreting in an Unstable Regime

Ryuichi Kurosawa^{1,a} and M. M. Romanova²

¹*Max-Planck-Institut für Radioastronomie, Auf dem Hügel, 69, 5312 Bonn, Germany*

²*Department of Astronomy, Cornell University, Ithaca, NY 14853-6801, USA*

Abstract. We discuss key observational signatures of Classical T Tauri stars (CTTSs) accreting through Rayleigh-Taylor instability, which occurs at the interface between an accretion disk and a stellar magnetosphere. In this study, the results of global 3-D MHD simulations of accretion flows, in both stable and unstable regimes, are used to predict the variability of hydrogen emission lines and light curves associated with those two distinctive accretion flow patterns. In the stable regime, a redshifted absorption component (RAC) periodically appears in some hydrogen lines, but only during a fraction of a stellar rotation period. In the unstable regime, the RAC is present rather persistently during a whole stellar rotation period, and its strength varies non-periodically. The latter is caused by multiple accreting streams, formed randomly due to the instability, passing across the line of sight to an observer during one stellar rotation. This results in the quasi-stationarity appearance of the RAC because at least one of the accretion stream is almost always in the line of sight to an observer. In the stable regime, two stable hot spots produce a smooth and periodic light curve that shows only one or two peaks per stellar rotation. In the unstable regime, multiple hot spots formed on the surface of the star, produce the stochastic light curve with several peaks per rotation period.

1 Introduction

Time-scales of the variability exhibited by Classical T Tauri stars ranges from seconds to decades (e.g., [1], [2]). The cause of the variability in different times-scales are likely associated with different physical mechanisms. Here, we concentrate on the variability that occurs in the time-scale of a stellar rotation or less. One obvious cause of the variability in this time-scale is a stellar rotation. For example, the flux modulations caused by stellar spots, and the obscuration of a stellar surface by a large-scale warped disk adjacent to the magnetosphere, which corotates with the star (e.g. [3–5]), are evidently related with a stellar rotation period.

An interesting possibility in which matter accretes onto the star via the magnetic Rayleigh-Taylor (RT) instability has been investigated in the theoretical studies by e.g., [6–8]. More recently, the global three-dimensional (3D) magnetohydrodynamic (MHD) simulations by e.g. [9–11] have shown that the RT instability induces accretions in multiple (a few to several) unstable vertically elongated streams or ‘tongues’ which penetrate the magnetosphere. They found that the corresponding time-scale of the variability induced by the instability is typically a few times smaller than the rotation

^ae-mail: kurosawa@mpifr-bonn.mpg.de

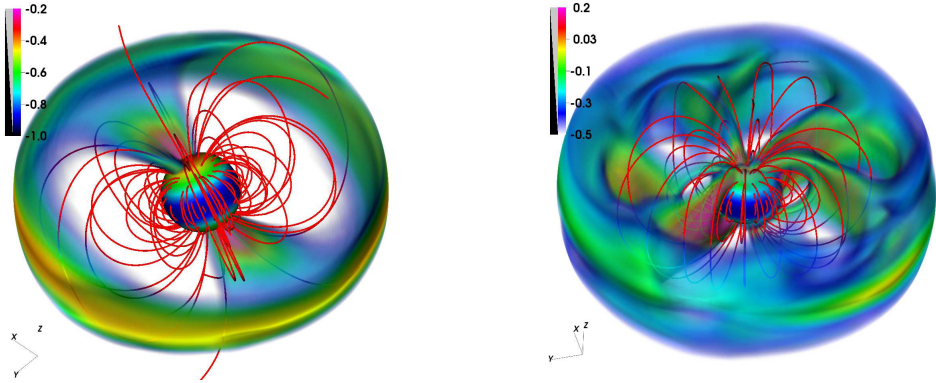


Figure 1. Examples of density distributions (volume renderings; in logarithmic scales; in arbitrary units) from the 3D MHD simulations of the accretion onto CTTs in a stable (left) and an unstable (right) regimes. Sample magnetic field lines are also shown (red lines).

	M_* (M_\odot)	R_* (R_\odot)	B_{eq} (G)	r_{cor} (R_*)	P_* (d)	Θ ($^\circ$)	α ($^\circ$)
Stable Case	0.8	2	10^3	5.1	4.3	30°	0.02
Unstable Case	0.8	2	10^3	8.6	9.2	5°	0.1

Table 1. Basic model parameters.

period of a star. In this study, we focus on the variability associated with the unstable accretion caused by the RT instability, and predict a few key observable signatures of CTTs accreting in this regime, by using radiative transfer models which incorporate the results from the 3D MHD simulations. The earlier MHD simulations (e.g. [9, 10]) have shown that the unstable tongues are randomly formed, and consequently hot spots on the stellar surface are also formed irregularly, in time, shapes and locations. This naturally leads to a formation of an irregular light-curve. Interestingly, such irregular light-curves are frequently observed in CTTs (e.g. [2, 4, 12]). Our aim here is to find unique signatures of CTTs accreting in the unstable regime by means of time-dependent modeling and analysis of emission line profiles of hydrogen.

The work presented here is based on the studies published in [13]. In Sec. 2, we briefly summarize our MHD and radiative transfer models. Our main results are presented in Sec. 3, and our main findings are given in Sec. 4.

2 Models

First, we calculate the matter flows in a global 3D MHD simulation with frequent writings of data (about 25 time-slices per stellar rotation and for 3 rotation periods). The *multiple time-slices* of the MHD simulation data are then used as the input of a separate 3D radiative transfer code to compute light curves and line profiles which can be compared with observations. The multiple time-slices allow us to follow the time evolution of the line profiles that occurs as a consequence of the dynamical nature of the accretion flows in the unstable regime. In earlier studies, we have used a similar procedure to

calculate line profiles of a star accreting in a stable regime by using only *a single time-slice* of MHD simulations in which the gas accretes in two ordered funnel streams [14]. More recently, we have performed a similar modeling for a star with realistic stellar parameters (i.e. V2129 Oph), and have found a good agreement between the model and the time-series observed line profiles [15].

We perform two separate numerical MHD simulations of matter flows with the parameters shown in Table 1, which are known to produce a stable and an unstable magnetospheric accretion (e.g. [10]). Examples of the magnetospheric accretion flows in both stable and unstable regimes are shown in Fig. 1. The simulations follow the accretion flows around a rotating star with a dipole magnetic field with the magnetic axis tilted from the rotational axis by an angle Θ . The rotational axis of the star coincides with that of the accretion disk. A viscosity term has been added to the model with a viscosity coefficient proportional to the α parameter (e.g. [16]). The detail studies on the criteria for the magnetic RT instability are presented in e.g., [6, 17, 18]. In general, with our simulation setup, we find the instability develops more easily when a system has a relatively smaller tilt angle (Θ), a larger viscosity (α) and a longer rotation period (P_*) (see Table 1).

For the calculations of hydrogen emission line profiles from the matter flow in the MHD simulations, we use the radiative transfer code TORUS (e.g. [19–21]). In particular, the numerical method used in the current work is essentially identical to that in [20]; hence, for more comprehensive descriptions of our method, readers are referred to the earlier papers. The basic steps for computing the line variability are as follows: (1) mapping the MHD simulation data onto the radiative transfer grid, (2) source function (S_ν) calculations, and (3) observed line profile calculations as a function of rotational phase. In step (1), we use an adaptive mesh refinement which allows for an accurate mapping of the original MHD simulation data onto the radiative transfer grid. The density and velocity values from the MHD simulations are mapped here. In step (2), we use a method similar to that of [22] in which the Sobolev approximation (e.g. [23]) is applied. The size and shapes of the hot spots, formed at the stellar surface at the bases of the accretion streams, are adjusted accordingly with the energy fluxes of the streams impacting on the stellar surface. The radiation from the hot spots are included in the level population and the observed flux calculations. In general, the light curves and line profiles are greatly influenced by the radiation from hot spots. We set the gas temperatures in the accretion funnels for both the stable and unstable cases to be between ~ 6000 K and ~ 7500 K. In all the variability calculations presented in this work, we adopt the intermediate inclination angle $i = 60^\circ$.

3 Results

The subsets of the time-series line profile calculations for $H\delta$, $\text{Pa}\beta$ and $\text{Br}\gamma$ are summarized in Fig. 2, with the rotational phase step $\Delta\phi = 0.16$, for the first rotation period. See [13] for the models of other hydrogen lines. The figure shows that the redshifted absorption components are prominent in $H\delta$ (in optical), $\text{Pa}\beta$ and $\text{Br}\gamma$ (in near-infrared) for both stable and unstable cases. For the stable accretion case, the redshifted absorption component (RAC) is visible in these lines during about a half of a rotational phase (between $\phi \sim 0$ and ~ 0.5). These phases approximately coincide with the phases when the upper accretion funnel stream is in front of the star (see Fig. 1), i.e. when the upper accretion funnel is in the line of sight of the observer to the stellar surface. A weak double-peak feature visible in $\text{Pa}\beta$ and $\text{Br}\gamma$ in the latter half of the rotational phase ($\phi \sim 0.5$ and ~ 1.0) is mainly caused by the ‘lack of emission’ from the gas moving at zero project velocity toward an observer. This is due to the geometrical effect (two distinct accretion streams) and the fact that the emission in $\text{Pa}\beta$ and $\text{Br}\gamma$ occurs near the base of accretion stream where the flow velocity is large ($\sim 200 \text{ km s}^{-1}$). At some phases, the gas at the inner edge of the accretion disk could also intersect the line of sight between the observer and the system, and causes a small amount of absorption near the line center since the

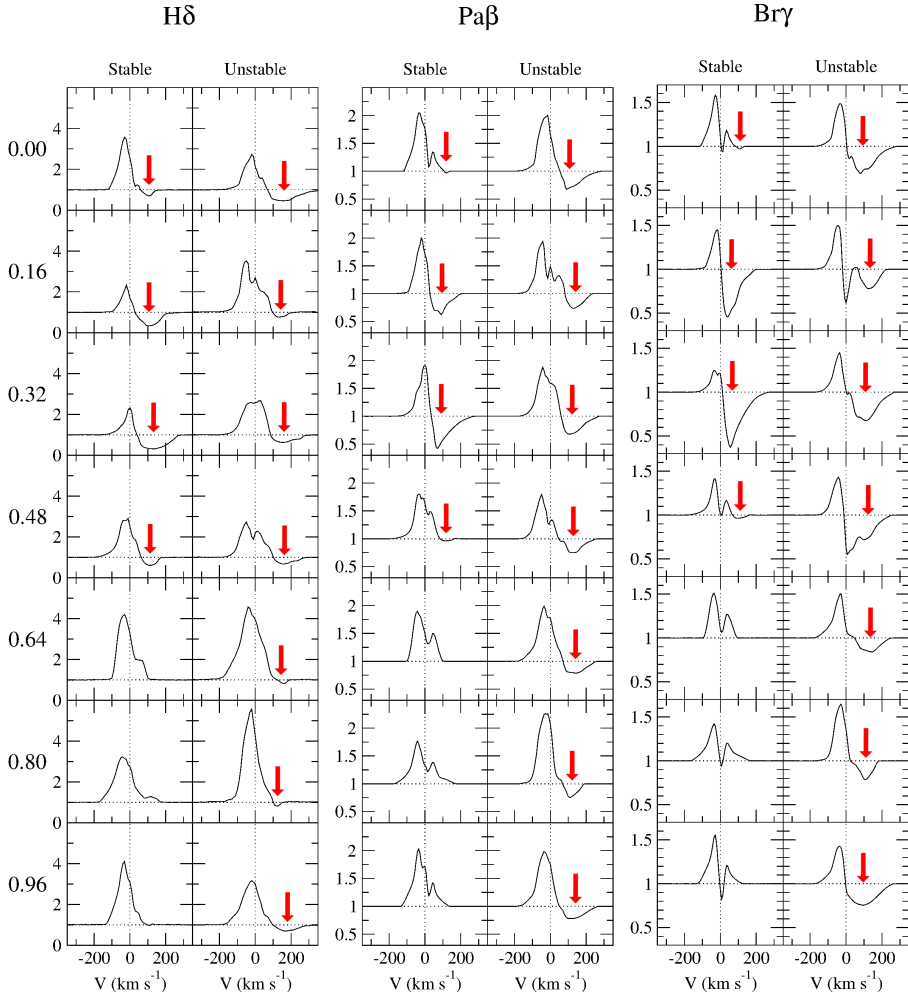


Figure 2. The time-series line profile models (solid) of H δ , Pa β and Br γ in the stable regime (left columns) and in the unstable regime (right columns) shown for different rotational phases (between 0 and 0.96). The rotational phase values are indicated in the leftmost column. All the profiles are computed with the system inclination angle $i = 60^\circ$. The red arrows indicate the presence and location of the redshifted absorption component.

intervening gas in the inner most part of the accretion disk is just rotating with a Keplerian velocity; hence, its projected velocity toward the observer would be around zero. This can also contribute to the double peaked appearances of Pa β and Br γ . For the unstable case, the RAC in H δ , Pa β and Br γ is present at almost all phases. This is due to the geometry of the accretion flows (see Fig. 1). The instability causes a few to several accretion streams to be present in the system at all times. Hence, at least one of the accretion streams or tongues is almost always in the line of sight of the observer to the stellar surface, and producing the RAC at all the rotational phases.

In Fig. 3, we summarize the light curves (monochromatic) computed at the frequencies around H δ along with their line EWs as a function of rotational phase (for three rotational phases) for both stable and unstable cases. While the light curve is very periodic for the stable case, it is quite irregular for

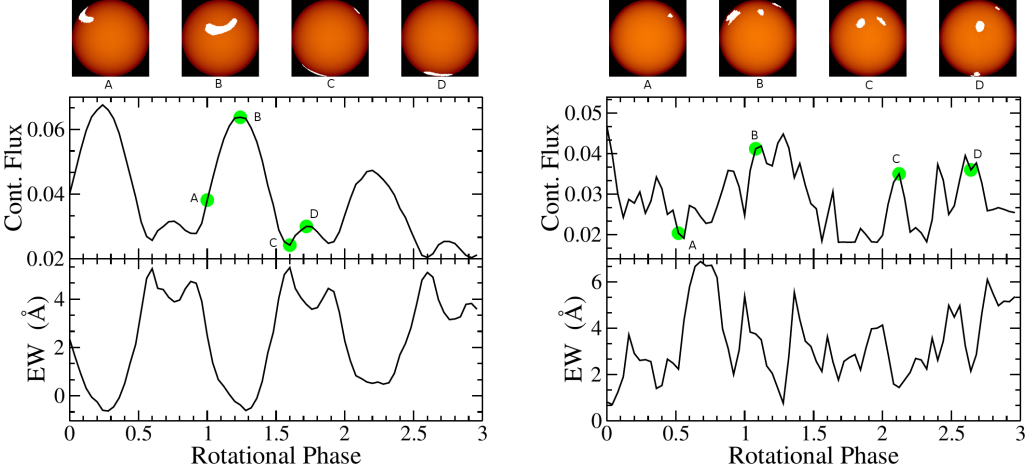


Figure 3. The maps of hot spots on the stellar surface at four different rotational phases, as seen by an observer (using the inclination angle $i = 60^\circ$). (top panels), the light-curves computed near the wavelength of $H\delta$ (middle panels) and the line equivalent widths (EWs) of model $H\delta$ profiles (lower panels) are shown for the stable (left panels) and unstable (right panels) regimes of accretions. The hot spots are shown for representative moments of time which are marked as green filled circles on the light curves.

the unstable case. In the stable case, the light curve clearly shows two maxima per period. These are caused by the rotation of the two hot spots on the stellar surface created by the two accretion streams (see Fig. 1). In an unstable regime, the light curves are irregular because the accretion streams/tongues form stochastically and deposit the gas onto the stellar surface in a stochastic manner. This results in the stochastic formation of hot spots which produce the stochastic light curve. The line EW variability curves are also influenced by the presence of hot spots since they contribute significantly to the total continuum flux. Since the lines are formed in the accretion stream which are formed irregularly, their EWs varies irregularly, as shown in Fig. 3. No clear periodicity is found in the light curve and the EW curve for the unstable case.

Interestingly, the regular/periodic and irregular light curves seen in our models are very similar to some of those found in the observations by e.g. [2] and [4]. Note that irregular light curves are found in about 39 per cent of the CTTs sample in [4]. No clear periodicity in the line variability is found in many CTTs. For example, in the observation of TW Hya, [24] found that the variability of $H\alpha$ and $H\beta$ are not periodic, and suggested the cause of the variability is intrinsic (e.g. changes in the mass-accretion rates) rather than the stellar rotation. In the studies of DR Tau by [25] and DF Tau by [26], no clear periodicity was found in their line variability observations. However, the line variability seen in these two objects may be also influenced by strong winds clearly present in some line profiles.

4 Summary

In this study, we find that the CTTs accreting in the unstable regime (due to the magnetic RT instability) would exhibit (1). irregular light curves and (2). variable but rather persistent redshifted absorption component in higher Balmer lines (e.g., $H\gamma$ and $H\delta$) and in some near-infrared hydrogen lines such as $\text{Pa}\beta$ and $\text{Br}\gamma$. Although an irregular curve could be also formed by stochastically occur-

ring flare events, the persistent redshifted absorption component is not expected to be associated in such events.

Acknowledgment

We thank the conference organizers, especially the chair, Prof. E. Bozzo for the excellent meeting. Resources supporting this work were provided by the NASA High-End Computing (HEC) Program through the NASA Advanced Supercomputing (NAS) Division at Ames Research Center and the NASA Center for Computational Sciences (NCCS) at Goddard Space Flight Center. The research was supported by NASA grants NNX10AF63G, NNX11AF33G and NSF grant AST-1008636.

References

- [1] W. Herbst, C.A.L. Bailer-Jones, R. Mundt, K. Meisenheimer, R. Wackermann, *A&A* **396**, 513 (2002)
- [2] S.M. Rucinski, J.M. Matthews, R. Kuschnig, G. Pojmański, J. Rowe, D.B. Guenther, A.F.J. Moffat, D. Sasselov, G.A.H. Walker, W.W. Weiss, *MNRAS* **391**, 1913 (2008)
- [3] J. Bouvier, K.N. Grankin, S.H.P. Alencar, C. Dougados, M. Fernández, G. Basri, C. Batalha, E. Guenther, M.A. Ibrahimov, T.Y. Magakian et al., *A&A* **409**, 169 (2003)
- [4] S.H.P. Alencar, P.S. Teixeira, M.M. Guimarães, P.T. McGinnis, J.F. Gameiro, J. Bouvier, S. Aigrain, E. Flaccomio, F. Favata, *A&A* **519**, A88 (2010)
- [5] M.M. Romanova, G.V. Ustyugova, A.V. Koldoba, R.V.E. Lovelace, *MNRAS* **430**, 699 (2013)
- [6] J. Arons, S.M. Lea, *ApJ* **207**, 914 (1976)
- [7] H.C. Spruit, R.E. Taam, *ApJ* **402**, 593 (1993)
- [8] L.X. Li, R. Narayan, *ApJ* **601**, 414 (2004)
- [9] M.M. Romanova, A.K. Kulkarni, R.V.E. Lovelace, *ApJ* **673**, L171 (2008)
- [10] A.K. Kulkarni, M.M. Romanova, *MNRAS* **386**, 673 (2008)
- [11] A.K. Kulkarni, M.M. Romanova, *MNRAS* **398**, 701 (2009)
- [12] W. Herbst, D.K. Herbst, E.J. Grossman, D. Weinstein, *AJ* **108**, 1906 (1994)
- [13] R. Kurosawa, M.M. Romanova, *MNRAS* **431**, 2673 (2013)
- [14] R. Kurosawa, M.M. Romanova, T.J. Harries, *MNRAS* **385**, 1931 (2008)
- [15] S.H.P. Alencar, J. Bouvier, F.M. Walter, C. Dougados, J.F. Donati, R. Kurosawa, M. Romanova, X. Bonfils, G.H.R.A. Lima, S. Massaro et al., *A&A* **541**, A116 (2012)
- [16] N.I. Shakura, R.A. Sunyaev, *A&A* **24**, 337 (1973)
- [17] M. Kaisig, T. Tajima, R.V.E. Lovelace, *ApJ* **386**, 83 (1992)
- [18] H.C. Spruit, R. Stehle, J.C.B. Papaloizou, *MNRAS* **275**, 1223 (1995)
- [19] T.J. Harries, *MNRAS* **315**, 722 (2000)
- [20] R. Kurosawa, M.M. Romanova, T.J. Harries, *MNRAS* **416**, 2623 (2011)
- [21] R. Kurosawa, M.M. Romanova, *MNRAS* **426**, 2901 (2012)
- [22] R.I. Klein, J.I. Castor, *ApJ* **220**, 902 (1978)
- [23] V.V. Sobolev, *Soviet Astronomy* **1**, 678 (1957)
- [24] J.F. Donati, S.G. Gregory, S.H.P. Alencar, J. Bouvier, G. Hussain, M. Skelly, C. Dougados, M.M. Jardine, F. Ménard, M.M. Romanova et al., *MNRAS* **417**, 472 (2011)
- [25] S.H.P. Alencar, C.M. Johns-Krull, G. Basri, *AJ* **122**, 3335 (2001)
- [26] C.M. Johns-Krull, G. Basri, *ApJ* **474**, 433 (1997)